Nanodiodes on a Digestible Substrate

Gwenhivir Wyatt-Moon, Ganapathy Saravanavel, Sanjiv Sambandan and Andrew J. Flewitt

Abstract
Biodegradable and edible electronics will need electronic components for signal modulation and wireless communication; hence, non-linear and high frequency components will be required. Here, a method to fabricate nanodiodes on isomalt (a sugar substitute) substrates is reported. Coplanar electrodes of Al and Au with nanogap separation were fabricated on top of isomalt through design of an adhesion lithography process specifically to accommodate the low melting point and high solubility of the substrate. Lateral diodes with rectification ratios of 10^3 were created by depositing indium gallium zinc oxide (IGZO) using a target with an atomic ratio of In_2O_3:Ga_2O_3:ZnO (1:1:1) on top of the electrodes without an annealing step.

Introduction

Digestible and biodegradable electronics have applications in personalized healthcare and environmental sustainability. Much of the research on edible electronics is focused on the materials and component parts necessary for a device that is fully safe to digest [1]–[3]. Unlike ingestible devices (which typically pass through the body without being broken down), the materials that these edible systems comprise of must all be nontoxic to humans. Communications systems in devices will need to be wireless with an external system collecting and evaluating data. [1]. Passive Radio frequency ID (RFID) tags, that do not require a power supply offer a solution, though frequency choice and antenna design are very important for successful penetration through human tissue to an external antenna [4]. To achieve this and to also for signal modulation, it is necessary to incorporate non-linear devices such as diodes and transistors.

In this paper we report the first diodes fabricated on a fully digestible isomalt (a sugar substitute) substrate (i.e. where the substrate would not pass through the body intact). Previous work has been carried out in developing other types of biocompatible substrates (i.e. cellulose) focusing on larger-size transistors [5]. This was made possible by designing an adhesion lithography (a-Lith) process specifically for this kind of substrate which is both soluble and has a very low melting point. This technique was originally developed to create a pair of planar electrodes separated by a small gap down to 3 nm in length [6][7].

The process presented in this work is almost dry, avoiding dissolution of the substrate, and does not employ annealing, which would melt the substrate. The planar nature of the electrodes removes unwanted pinhole effects that may otherwise be formed in typical diode sandwich structures as a result of the roughness of the isomalt substrate.

Defining the toxicity of materials through digestion is complex. For the materials used within these diodes a couple of factors must be taken into consideration. Different compounds of materials produce different effects on the body and while the materials used here (Al, Au, In, Ga and Zn) have shown little toxicity through the gastrointestinal tract [8], compounds and how they are converted within the body can change these effects, though typically metal oxides are not more toxic than their metal counterparts [9]. Al is commonly found in both drinking water and food and Au is already used as a food additive (E175). With the absolute amount of each of these materials kept at a low level by using thin films of >80 nm thickness, the metals used as electrodes in these devices should be well below the daily safe exposure limits for humans [10][11]. The semiconductor used with these devices is indium gallium zinc oxide (IGZO). This material requires further studies to determine if there is any toxic effect on humans through digestion, so cannot yet be described as a digestible material.

SUBSTRATE AND DEVICE FABRICATION

Fabrication of Isomalt substrates was developed from previous work [12]. Isomalt pellets were heated to their melting point of about 200 ºC with continuous stirring. The melt was then cooled to around 120 ºC to form a viscous gel that was sandwiched between two polydimethylsiloxane (PDMS) sheets which were in turn sandwiched between optically smooth glass plates. The application of a uniformly distributed force on the glass plates allowed for the viscous isomalt gel to spread uniformly to a desired thickness. The entire setup was then cooled to room temperature and the isomalt was then extracted as a smooth, clear substrate.

Fig. 1(a) is an image of a typical isomalt substrate of roughly 25 mm in diameter. There is long range (mm) height variability on the surface of the substrate due to the fabrication process. A 20 × 20 µm AFM topographic micrograph of the surface (Fig. 1(b)) shows an RMS roughness of 3.4 nm and height differences of over 100 nm which is to be expected in substrates manufactured at very low cost and with limited control of surface morphology. This variability in the surface makes it difficult to create thin film diodes using typical sandwich structures, as pinholes and device shorting normally become an issue for such large-scale asperities. However, the isomalt is smooth on a small-scale, meaning lateral nanoscale devices are statistically unlikely to be compromised.

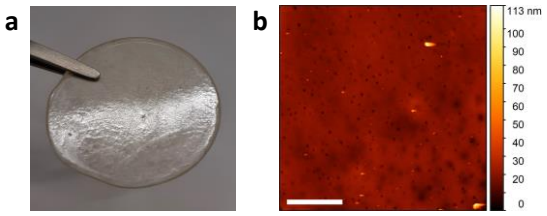

Fig. 1. (a) Photograph of the isomalt substrate (diameter ~25 mm). (b) AFM topological micrograph of the isomalt surface, Scale bar: 5 µm.

To fabricate nanogap electrodes on isomalt, a specially designed a-Lith process was used (detailed in results). 40 nm Al (99.9% purity) was deposited via thermal evaporation at 0.8 nm s^{-1} with a base pressure of 2×10^{-6} mbar. The Octadecylphosphonic acid (ODPA) was dissolved into IPA (99% purity) at a ratio of 30 mg : 50 ml. and stirred for 2 hours. 5 nm Cr and 35 nm Au (99.9% purity) were then deposited on top of the substrate using the same evaporator and base pressure at rates of 0.1 nm s^{-1} and 0.08 nm s^{-1}, respectively (Fig. 2(a)). Tape (3M® polyester tape (part no. T1350Y12)) was then placed on the gold layer and peeled. The Cr/Au layer was selectively removed from areas on the substrate where there was the SAM and remained in the areas where it was in contact with the isomalt. The fracture of the Au at the Al-SAM-substrate interface resulted in a nanogap forming laterally between the two metals (Fig. 2(b)).

IGZO deposition was carried out via by rf-magnetron sputtering (CCR GmbH) with an IGZO target (In_2O_3:Ga_2O_3:ZnO (1:1:1), Pi-Kem; 99.99% purity) and the chamber was pumped down for 2 hours prior to IGZO deposition for 15 mins. Sputtering was performed at 75 W power with 19 sccm of Ar (BOC Gases; 99.999%) at a base pressure of 3.8×10^{-4} mbar.

AFM topological micrographs were taken using intermittent contact mode on an Agilent N9605A. A Zeiss Olympus optical microscope was used for optical images via NIS-Elements Software (Nikon Metrology).

Electrical characterization was preformed using an Agilent B1500A semiconductor parameter analyzer. The Au electrodes were grounded with the voltage applied to the Al electrodes. All measurements were carried out under ambient conditions.

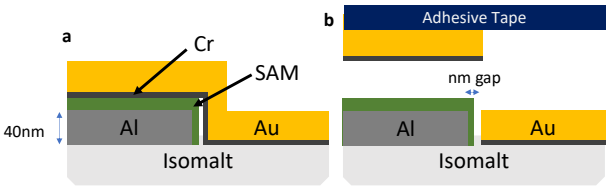

Fig. 2 Schematic of the adhesion lithography process on top of isomalt. (a) Al is deposited then the self-assembled monolayer (SAM) is attached selectively to the Al and Cr/Au (M2) deposited on top. (b) Adhesive tape is attached to the sample and then peeled off to remove the Cr/Au (M2) on top of the SAM. Leaving a nanogap between the electrodes.

RESULTS AND DISCUSSION

Traditional patterning techniques for metals (e.g. photolithography) were not able to be used with this process due to the solubility and low melting temperature of the isomalt substrate, hence a shadow mask was used for patterning M1. For the first iteration of the a-Lith process 40 nm Al was deposited via thermal evaporation (Fig. 3(a)). The substrate was then placed upside down in a vessel and raised up from the base using glass slides. It was then partially submerged by 1 mm into an ODPA/IPA solution to minimize exposure of the isomalt to a solution.

As shown in Fig. 3(b) the Al deposited via thermal evaporation was damaged by the SAM immersion and began flaking away from the surface. M2 (Cr/Au) was then deposited and peeled using a tape adhesive with low adhesive force. The peel step of the second metal was partially successful (Fig. 3(c)) with M2 being removed from on top of M1, but there are large gaps and damage to both metals. This suggests the SAM successfully attached to M1, but the substrate and M1 were too damaged to allow for formation of nanogaps between the two metals. The microscope image in Fig. 3(d) shows that in some of the areas where M1 has been damaged by the ODPA solution, small flakes of gold can be seen.

Al deposited via a metal sputter coater was also tested as the M1 layer. The same shadow mask was employed for patterning. M1 from this deposition was less damaged by the SAM immersion (Fig. 3(e)), but due to shadowing, the resulting gaps between the two metal layers were on the order of a 100 µm (Fig. 3(f)).

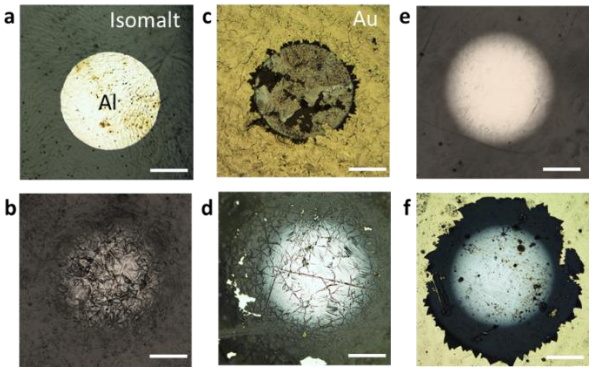

Fig. 3 Optical microscope images showing metal tests on isomalt using standard process. (a) 40nm Al is deposited via thermal evaporation. (b) Al after SAM immersion of 10 mins showing damage to Al. (c) and (d) Immersion samples after Cr/Au deposition showing partial success of adhesion lithography (e) Al deposited via shadow mask and sputtering (f) Sputtered sample after adhesive peel showing effect of shadow mask. Scale bars: 250 µm.

To stop damage to the electrodes and substrate, a new SAM coating method was employed. The substrate was held at a slight (roughly 10°) angle from vertical and ~2ml SAM solution was washed over the surface using a pipette for 1s; this was immediately dried with compressed air. It was expected that the SAM coating would be somewhat compromised as it had not had optimal time to attach to M1 [13] and annealing

to aid monolayer uniformity was not possible due to the risk of melting the isomalt [14]. However, SAM coating does appear to be sufficient for the process. M2 was subsequently deposited and peeled using adhesive tape. The resultant structures (Fig. 4(a)&(b)) show a much more uniform gap between the two metals with the gap not visible under an optical microscope. Both electrodes are conforming to the shape of the substrate and there is little or no damage to the Al due to the new SAM deposition process.

The I-V characteristics (Fig. 4(c)) across the two electrodes for 3 different devices show that the electrodes are electrically isolated, with currents in pAs due to noise. To confirm that success of this process was due to the SAM attachment on the Al, Al samples that had not undergone the SAM wash step were deposited with Cr/Au and then peeled. The peel step either removed the Al from the isomalt (Fig. 4(d)) or did not remove any of the Cr/Au (Fig. 4(e)).

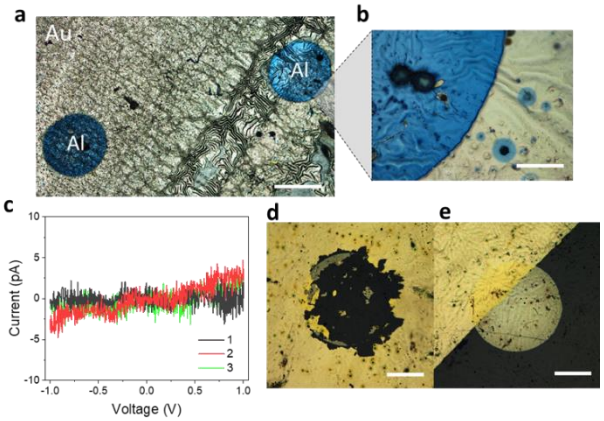

Fig. 4 (a) Al/Au nanogap electrodes. The Al is not damaged, and the Au has been removed from on top of the Al (Scale bar: 500 µm) (b) A further zoom showing the gap between the Al and Au, the gap cannot be resolved by the optical microscope (Scale bar: 50 µm). (c) I-V characteristics across the gap for three devices showing the electrical isolation of the two electrodes. (d) and (e) Samples peeled without the SAM wash showing either damage and removal of the Al or no removal of the Au from on top of the Al. (Scale bars: 250 µm).

A semiconductor material was then deposited on top of the electrodes to make Schottky diodes (diode schematic figure 5(a)). However, due to the isomalt substrate having a low melting point, the material could not be annealed, or solution processed, so a sputtered material, amorphous (a-)IGZO, was chosen. a-IGZO is a transparent semiconductor that has good electron mobility even in its amorphous state [15]. Techniques shown to improve device properties for Schottky diodes include tuning the amount of O_2 added to the sputtering chamber and carefully selecting the electrode materials [16]–[21].

The IGZO was deposited using a target with an atomic ratio of In_2O_3:Ga_2O_3:ZnO (1:1:1) and first deposited on devices of the same geometry on a glass substrate to allow for process optimization. The I-V characteristics shown in Fig. 5(b) possess some hysteresis and a rectification ratio of 10^3. These devices do not have as high a performance compared to previous work where a-IGZO devices on glass were annealed at 200 °C and had a rectification ratio of 10^4 with no hysteresis but do show good diode like behavior without the need for annealing [22]. The hysteresis in these devices is due to a lack of annealing and is likely due to defects in the IGZO film.

The optimized a-IGZO was then deposited onto the isomalt electrodes. I-V characteristics are also shown in Fig. 5(b). The devices have a rectification ratio of 10^3 and a small amount of hysteresis (~0.1 V) at positive biases with less hysteresis in the off current as compared to the glass devices. This difference is likely due to the distinct interfaces formed on the different types of substrate. For 5 devices measured on the same isomalt substrate (see Fig. 5(b) inset) the reverse current at -2 V ranged between -6 pA and -30 pA and the forward current at 2 V between 180 nA and 910 nA. This variation in current is likely due to slight irregularities in the nanogap size. The devices on isomalt have a slightly lower current than those on glass

for the same nominal gap length (nanogap), but similar rectification ratios. This is due to slightly different device geometries (electrode shape) on the isomalt substrate as compared to the glass. Calculating performance parameters using standard diode equations gives unrealistic values (e.g.a idealities factor of ~8-9) This is because of transport mechanisms, such as tunneling, caused by the nanoscale dimension of the devices, also effecting device characteristics.

Lateral IGZO devices on isomalt were also fabricated with ~150 µm sized gaps between them defined by the lift-off process at the same time as the nanogap devices. The I-V characteristics for these larger gap devices, also shown in Fig. 5(b), show no rectification with a slightly larger reverse current compared to the forward current. This proves that the ability for these devices to rectify is due to the nanogap between the electrodes and shows that techniques which can achieve this, like a-Lith, are required for diode devices to be created on isomalt.

CONCLUSION

Nonlinear devices will be useful for communication in digestible electronics. Planar nanogap a-IGZO diodes on isomalt (a digestible and biodegradable substrate) were fabricated. All the fabrication steps for the devices were carried out at room temperature, wet processing was reduced from hours to a couple of seconds and peeling step was carried out with a dry adhesive tape to minimize damage to the isomalt substrate. The resultant diodes had a good rectification ratio of 10^3 with little variability across devices. The ability to create these diodes was only successful due to the nanoscale feature sizes and planar structure of the a-Lith fabricated electrodes.

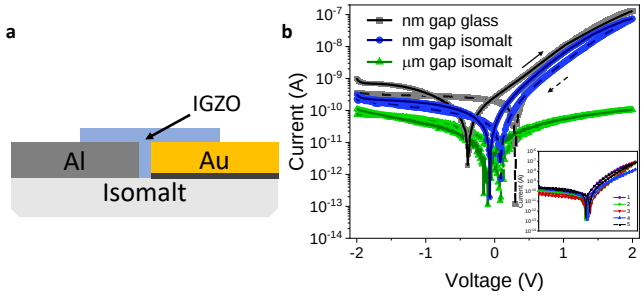

Fig. 5 (a) a 2D schematic of the device (b) Semi log plot of I-V characteristics of Al/Au IGZO diodes with no annealing: glass nm gap device and nm and µm gap isomalt devices. Inset: I-V of 5 devices on the same substrate.

REFERENCES

[1] W. Xu, H. Yang, W. Zeng, T. Houghton, X. Wang, R. Murthy, H. Kim, Y. Lin, M. Mignolet, H. Duan, H. Yu, M. Slepian, and H. Jiang, "Food-Based Edible and Nutritive Electronics," Adv. Mater. Technol., vol. 2, no. 11, pp. 1–7, 2017, doi: 10.1002/admt.201700181.

[2] A. S. Sharova, F. Melloni, G. Lanzani, C. J. Bettinger, and M. Caironi, "Edible Electronics: The Vision and the Challenge," Adv. Mater. Technol., vol. 6, no. 2, 2021, doi: 10.1002/admt.202000757.

[3] Y. Wu et al., "Edible and Nutritive Electronics: Materials, Fabrications, Components, and Applications," Adv. Mater. Technol., vol. 5, no. 10, pp. 1–28, 2020, doi: 10.1002/admt.202000100.

[4] C. Steiger, A. Abramson, P. Nadeau, A. P. Chandrakasan, R. Langer, and G. Traverso, "Ingestible electronics for diagnostics and therapy," Nat. Rev. Mater., vol. 4, no. 2, pp. 83–98, Feb. 2019, doi: 10.1038/s41578-018-0070-3.

[5] Pedro I. C. Claro, Inês Cunha, Rafaella T. Paschoalin, Diana Gaspar, Kelvi Miranda, Osvaldo N. Oliveira, Jr., Rodrigo Martins, Luís Pereira, José M. Marconcini, Elvira Fortunato, and Luiz H. C. Mattoso, "Ionic Conductive Cellulose Mats by Solution Blow Spinning as Substrate and a Dielectric Interstrate Layer for Flexible Electronics" ACS Appl. Mater. Interfaces, vol. 13, no. 22, pp. 26237−26246, May, 2021, doi: 10.1021/acsami.1c06274

[6] D. J. Beesley, J. Semple, L. K. Jagadamma, A. Amassian, M. A. McLachlan, T. D. Anthopoulos and J. C. deMello, "Sub-15-nm patterning of asymmetric metal electrodes and devices by adhesion lithography," Nat. Commun., vol. 5, no. 1, p. 3933, Sep. 2014, doi: 10.1038/ncomms4933.
[7] S. Luo, A. Mancini, R. Berté, B. H. Hoff, S. A. Maier, and J. C. de Mello, "Massively Parallel Arrays of Size-Controlled Metallic Nanogaps with Gap-Widths Down to the Sub-3-nm Level," Adv. Mater., vol. 33, no. 20, 2021, doi: 10.1002/adma.202100491.
[8] G. F. Nordberg, B. A. Fowler, and M. Nordberg, Eds., Handbook on the Toxicology of Metals. Academic Press, 2014.
[9] K. S. Egorova and V. P. Ananikov, "Toxicity of Metal Compounds: Knowledge and Myths," Organometallics, vol. 36, no. 21, pp. 4071–4090, Nov. 2017, doi: 10.1021/acs.organomet.7b00605.
[10] Scientific Opinion of the Panel on Food Additives, Flavourings, Processing Aids and Food Contact Materials on a request from European Commission on Safety of aluminium from dietary intake. EFSA J., 754, pp. 1–34, 2008, doi: 10.2903/j.efsa.2008.754.
[11] EFSA ANS Panel, "Scientific Opinion on the re-evaluation of gold (E 175) as a food additive," EFSA J., vol. 14, no. 1, 2016, doi: 10.2903/j.efsa.2016.4362.
[12] G. Saravanavel, S. John, G. K. R., G. Wyatt-Moon, A. Flewitt, and S. Sambandan, "Edible Resonators," Feb. 2022, [Online]. Available: http://arxiv.org/abs/2202.13782.
[13] C. Meltzer, H. Yu, W. Peukert, and B. Braunschweig, "Molecular structure of octadecylphosphonic acids during their self-assembly on α-Al2O3(0001)," Phys. Chem. Chem. Phys., vol. 20, no. 29, pp. 19382–19389, Jul. 2018, doi: 10.1039/c8cp02391c.
[14] E. S. Gawalt, M. J. Avaltroni, N. Koch, and J. Schwartz, "Self-assembly and bonding of alkanephosphonic acids on the native oxide surface of titanium," Langmuir, vol. 17, no. 19, pp. 5736–5738, Jul. 2001, doi: 10.1021/la010649x.
[15] K. Nomura, H. Ohta, A. Takagi, T. Kamiya, M. Hirano, and H. Hosono, "Room-temperature fabrication of transparent flexible thin-film transistors using amorphous oxide semiconductors," Nature, vol. 432, no. 7016, pp. 488–492, Nov. 2004, doi: 10.1038/nature03090.
[16] H. Yabuta, M. Sano, K. Abe, T. Aiba, T. Den, H. Kumomi, K. Nomura, T. Kamiya, and H. Hosono, "High-mobility thin-film transistor with amorphous InGaZnO4 channel fabricated by room temperature rf-magnetron sputtering," Appl. Phys. Lett., vol. 89, no. 11, p. 112123, Sep. 2006, doi: 10.1063/1.2353811.
[17] D. H. Lee, K. Nomura, T. Kamiya, and H. Hosono, "Diffusion-Limited a-IGZO/Pt Schottky Junction Fabricated at 200◦C on a Flexible Substrate," IEEE Electron Device Lett., vol. 32, no. 12, pp. 1695–1697, Dec. 2011, doi: 10.1109/LED.2011.2167123.
[18] L. Du, J. Zhang, Y. Li, M. Xu, Q. Wang, A. Song and Q. Xin, "High-Performance Flexible Schottky Diodes Based on Sputtered InGaZnO," IEEE Trans. Electron Devices, vol. 65, no. 10, pp. 4326–4333, Oct. 2018, doi: 10.1109/TED.2018.2864165.
[19] J. Zhang, H. Wang, J. Wilson, X. Ma, J. Jin, and A. Song, "Room Temperature Processed Ultrahigh-Frequency Indium-Gallium–Zinc-Oxide Schottky Diode," IEEE Electron Device Lett., vol. 37, no. 4, pp. 389–392, Apr. 2016, doi: 10.1109/LED.2016.2535904.
[20] J. Zhang, Y. Li, B. Zhang, H. Wang, Q. Xin, and A. Song, "Flexible indium–gallium–zinc–oxide Schottky diode operating beyond 2.45 GHz," Nat. Commun., vol. 6, no. 1, p. 7561, Nov. 2015, doi: 10.1038/ncomms8561.
[21] D. Lee, J. W. Park, K. Kim, H. Kim, and Y. S. Kim, "Strategies for High-Performance Amorphous Indium-Gallium-Zinc Oxide Schottky Contact via Defect-Induced Physical Interface Modification," ACS Appl. Electron. Mater., vol. 3, no. 4, pp. 1864–1872, 2021, doi: 10.1021/acsaelm.1c00104.
[22] G. Wyatt-Moon, K. M. Niang, C. B. Rider, and A. J. Flewitt, "Air Stable Indium-Gallium-Zinc-Oxide Diodes with a 6.4 GHz Extrinsic Cutoff Frequency Fabricated Using Adhesion Lithography," IEEE Electron Device Lett., vol. 41, no. 1, pp. 175–178, Jan. 2020, doi: 0.1109/LED.2019.2953982.